Available online at www.sciencedirect.com
SCIENCE DIRECT®
Journal of Photochemistry and Photobiology A: Chemistry 171 (2005) 251–256
Journal of Photochemistry and Photobiology A:Chemistry
www.elsevier.com/locate/jphotochem

Solution photolysis of ferrocene into Fe-based nanoparticles

Akihiko Ouchi[a], Tatsuo Tsunoda[a], Zdeněk Bastl[b], Miroslav Maryško[c], Vladimír Vorlíček[c], Jaroslav Boháček[d], Karel Vacek[e], Josef Pola[e,*]

[a] *National Institute of Advanced Industrial Science and Technology, AIST, Tsukuba, Ibaraki 305-8565, Japan*
[b] *J. Heyrovský Institute of Physical Chemistry, Academy of Sciences of the Czech Republic, 18223 Prague 8, Czech Republic*
[c] *Institute of Physics, Academy of Sciences of the Czech Republic, 18040 Prague, Czech Republic*
[d] *Institute of Inorganic Chemistry, Academy of Sciences of the Czech Republic, 25068 Řež, Czech Republic*
[e] *Laser Chemistry Group, Institute of Chemical Process Fundamentals, Academy of Sciences of the Czech Republic, 16502 Prague 6, Czech Republic*

Received 6 September 2004; received in revised form 22 October 2004; accepted 28 October 2004
Available online 7 December 2004

Abstract

ArF laser photolysis of ferrocene in hexane yields hydrocarbons produced from both intermediate cyclopentadienyl radical and the solvent, and it affords chemical solution-phase deposition of Fe-based particles which consist of a Fe core and oxidized outer layers. These particles are covered with a carbonaceous polymer, they have a characteristic UV spectrum and show both a ferromagnetic ($T = 5$ K) and superparamagnetic ($T > 120$ K) behaviour.

Keywords: Ferrocene; Laser photolysis; Fe-based nanoparticles

1. Introduction

UV laser-induced multiphoton dissociation of ferrocene in the gas phase is known [1(a)–(d)] to yield iron atoms and presumably [2] cyclopentadienyl radical. The feasible gas-phase production of high density of Fe atoms by ArF laser photolysis of ferrrocene has been recently used for the deposition or Fe and Fe/C nanoparticles [3], the latter obviously originating from the cyclopentadienyl radical decomposition.

This facile gas-phase photochemical decomposition contradicts with ferrocene photochemical stability [4] in non-chlorinated solvents under conditions of conventional low-intensity UV radiation, which suggested the use of ferrocene and its derivatives as protective ultraviolet absorbers [5].

The liquid-phase UV photolysis of ferrocene at high laser irradiation intensity has not been yet studied, despite that the solvent could provide a cooling effect to the produced fragments and the reaction is of interest in view of possible cyclopentadienyl radical-induced polymerisation, which might create suitable conditions for formation of iron nanoparticles incorporated in a polymer. These materials are finding recent interest [6].

In this paper, we show that the photolysis of ferrocene in non-polar solvent can be accomplished by using an intense ArF laser radiation and that it results in the formation of Fe nanoparticles that are covered with a carbonaceous phase. We deduce on the fate of the photolytically produced cyclopentadienyl radical in solution and show that the deposited particles possess characteristic UV–vis spectrum and have temperature-dependent magnetic behaviour.

2. Experimental part

Solutions of ferrocene (Aldrich, 98%), 1.3–11.6 × 10^{-3} molar in hexane (Cica-Reagent for spectroscopy), were stirred by a magnetic bar in a 4 ml quartz cell or in a 50 ml quartz tube under Ar and irradiated with an ArF (Lambda Physik CPX 200) laser with a repetition frequency of 10 Hz. The irradiation time was several minutes (experiments in the quartz cell) and 2–3 h (experiments in the quartz tube). The

* Corresponding author. Tel.: +420 2 20390308; fax: +420 2 20920661.
E-mail address: pola@icpf.cas.cz (J. Pola).

1010-6030/$ – see front matter © 2004 Elsevier B.V. All rights reserved.
doi:10.1016/j.jphotochem.2004.10.020

laser energy effective on the incident area was 100 mJ on 1 cm^2 (the cell) and 300 mJ on 5 cm^2 (the tube). The progress of the ferrocene photolysis conducted in the cell was followed through UV spectra (a Shimadzu UV-2100 spectrometer).

After the irradiation, particles formed during the photolysis in the tube were centrifuged from the solution, washed with hexane and again centrifuged. This procedure was repeated three times and the obtained solid was treated under high vacuum.

The centrifuged solutions freed of the particles were analysed on a gas chromatograph (a Gasukuro Kogyo 370 chromatograph, a 2 m SUS Unipak S column, programmed temperature 30–150 °C, flame-ionization detector) connected with a Shimadzu CR 5A Chromatopac data processor and on a GS/MS spectrometer (a Shimadzu QP 5050 mass spectrometer, 60 m capillary column Neutrabond-1, programmed temperature 30–200 °C). The detected photolytic products were identified by using the NIST library.

The solid was analyzed by Raman, electron paramagnetic resonance (EPR) and X-ray photoelectron (XP) spectroscopy and by electron microscopy and examined for their magnetic properties.

The X-ray Fe 2p, C 1s and O 1s photoelectron spectra of the powders (as prepared and after mild sputtering with argon ions; $E = 5$ keV, $I = 40$ μA, 5 min) were measured using a VG ESCA3 MkII electron spectrometer with a base pressure better than 10^{-7} Pa and using Al Kα radiation (1486.6 eV) for electron excitation. The surface composition of the deposited film was determined by correcting the spectral intensities for subshell photoionization cross-sections [7].

The Raman spectra were recorded on a Renishaw microscope (Ramascope, model 1000). Exciting beam of an Ar-ion laser was defocused to diminish the heating of the samples.

The EPR spectra were acquired on a cw X-band spectrometer (100 kHz magnetic field modulation and 1 mW of microwave power) at room temperature in air using internal (Mn^{2+}) and external (TEMPOL) standards.

TEM analysis was conducted on a JEOL (JEM-2010 F) at 200 kV and at a Philips 201 transmission electron microscope at 80 kV. Process diffraction [8] was used to evaluate and compare measured electron diffraction patterns with XRD diffraction database [9].

Magnetization studies on the powder sample were performed in the temperature range 5–300 K using a SQUID magnetometer (MPM-5S, Quantum Design). The measurements were made either in zero-field cooling (ZFC) or field-cooling (FC) conditions.

Elemental analysis of the powder has been performed on a Perkin-Elmer 2400 analyzer.

3. Results and discussion

Ferrocene shows a strong absorption at the region of the ArF laser emission at 193 nm corresponding to the ligand-to-metal charge transfer transition [10].

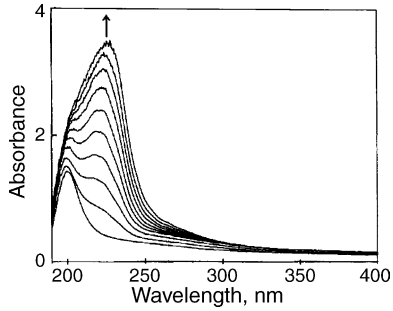

Fig. 1. ArF laser irradiation of 1.3×10^{-3} M hexane solution of ferrocene in the cell. (Fluence 100 mJ cm^{-2}; the built up of the absorption curves corresponds to the irradiation for 0–420 s with an increment of 70 s).

3.1. Photolysis

The ArF laser irradiation of the ferrocene solutions in hexane in the quartz cell results in the formation of tiny bubbles that are observed to arise from the irradiated spot behind the front cell wall. This indicates formation of gaseous products expelled from the solution and is in keeping of the photolysis proceeding just behind the quartz–liquid interface. (We note that the formation of bubbles is not observed with the laser irradiation of hexane itself). Gradual changes in the UV spectral pattern of the irradiated solution (Fig. 1) within the first several minutes irradiation are compatible with the formation of photolytic products having absorption at ∼230 nm. Similar absorption pattern—an intense band at ∼230 nm tailing to 290 nm was also observed with longer irradiation times.

The prolonged ArF laser irradiation of the ferrocene solutions in hexane in the quartz tube allows a slow formation of dark yellow particles that remain suspended in the stirred solution. After the irradiation and stirring is ceased, the particles slowly descend to the tube bottom. Thus, ca. 2–3 mg of a dark powder can be obtained with irradiation times as long as 150 min and this corresponds to photochemical yield lower than 10^{-3} provided that the iron content in the dark particles is ca. 66 wt.% (see later). The very low photochemical efficiency of ferrocene decomposition is compatible with a solvent effect. The used irradiation intensities are in the range of those inducing [1(c)] the gas-phase photolysis via two-photon absorption, which was assumed to occur via sequential elimination of the cyclopentadienyl radicals. We surmise that the second photon absorption is made less feasible through an energy transfer to solvent molecules and that the photolysis takes place as a one photon-induced process [1(a)]. (Cleavage of both Fe-ligand bonds requires 593 kJ $mole^{-1}$ [1(c),11] and the energy of the 193 nm photons is 620 kJ $mole^{-1}$).

Although assumed as a plausible transient species in the gas-phase flash photolysis of ferrocene [2], the cyclopentadienyl radical [12] has never been detected in the laser photolyses of ferrocene in the gas and liquid phase. Our search on the final photolytic hydrocarbon products was therefore aimed at understanding the fate of the presumed C_5H_5 transient.

Table 1
Gaseous products of ArF laser photolysis[a]

Irradiation of	Gaseous products(relative mole %)				
	CH_4	C_2H_6	C_2H_4	C_3H_8	C_2H_2
Ferrocene (s)	0.22	–	0.12	–	1.00
Hexane (l)	0.80	0.33	1.20	0.05	1.00
Ferrocene solution in hexane	0.87	0.33	2.50	0.11	1.00

[a] Fluence 60 mJ cm^{-2}.

The gaseous products escaping from the solution were identified as methane, ethylene and acetylene (the main product) along with ethane and propane (minor products). Independent irradiation of solid ferrocene and hexane revealed that the former yields mostly acetylene and the latter yields methane, ethane, ethylene, and acetylene as main gaseous products (Table 1). These observations allow to conclude that the hydrocarbons observed at the laser photolysis of the solution of ferrocene are produced both from ferrocene and the solvent.

The chemical changes monitored in the solutions irradiated in the quartz tube after 20 and 120 min by GC/MS revealed the presence of traces of 3-pent-1-yne, 1,3-butadiene, benzene, toluene, xylenes, ethylbenzene, 1-methyd-1H-indene (*m*/*z*, intensity in (%): 130, 88; 129, 100; 128, 31; 127, 18; 115, 79; 77, 14; 64, 17; 65, 23; 51, 36; 39, 38), 3a,4,7,7a-tetrahydro-4,7-methano-1H-indene (dicyclopentadiene) (*m*/*z*, intensity: 132, 11; 66, 100; 65, 13; 39, 14) and methylferrocene (*m*/*z*, intensity: 201, 18; 200, 100; 134, 54; 121, 29; 56, 56).

The presence of these compounds gives indirect evidence on the transient occurrence of CH_3 and C_5H_5 radicals. We assume that the latter mostly (i) decomposes to acetylene, some highly unsaturated species and carbon (see later) and (ii) abstracts H to yield cyclopentadiene which undergoes [13] both photo-cyclodimerization to the observed dicyclopentadiene and (Diels–Alder) polymerization reactions [14]. Although we could not detect cyclopentadiene by GC/MS, its temporary formation in the solution is manifested through its absorption at 237 nm [15] (Fig. 1).

The absence of 9,10-dihydrofulvene (the product of recombination of cyclopentadienyl radical) and/or its isomers [16] but not of dicyclopentadiene (i.e. cyclopentadiene) is in keeping with the presumed sequential cleavage of the C_5H_5 radical (one photon mechanism [1(c)]) and preferential H abstraction by this species. We admit, however, that 9,10-dihydrofulvene can disappear due to polymerization reactions.

Acetylene, methane, butadiene and the aromatic compounds are the known [17] products of thermal decomposition of cyclopentadiene and they can originate not only from the C_5H_5 radical but also from cyclopentadiene (formed from C_5H_5 radical by H-abstraction). Their formation together with that of carbon (see later) indicates that the energy liberated in the C_5H_5–Fe bond cleavage is transferred into the internal degrees of freedom of the C_5H_5 fragment and that the solvent does not provide efficient cooling of the hot C_5H_5 species. This feature is favorable to fragments decomposition and polymerization.

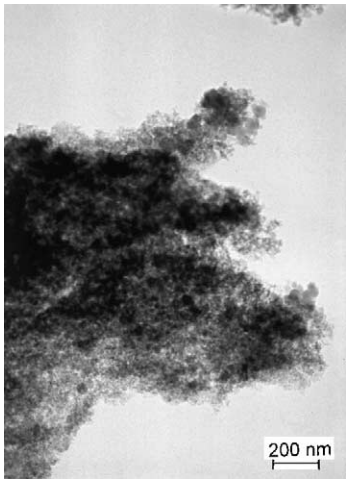

Fig. 2. TEM image of the powder.

3.2. Properties of deposited particles

The particles have a dark yellow colour when suspended in solution and form a dark (black) powder when they are collected together after solvent removal. The TEM examination of the powder revealed (Fig. 2) that the powder is composed of ca. 10 nm-sized or larger particles agglomerated into more voluminous bodies. Their elemental analysis reveals 31.2 wt.% of carbon and 3.2 wt.% of hydrogen, which implies a high content of Fe (see later).

Their surface stoichiometry calculated from the XP spectra intensities assuming the homogeneous sample is $Fe_{1.0}C_{31.0}O_{12.0}$ (sample as received) and $Fe_{1.0}C_{2.7}O_{0.9}$ (sample sputtered by Ar ions). The Fe 2p spectrum of the powder (Fig. 3a) before ion sputtering shows the presence of most likely Fe_3O_4 iron oxide [18,19] with binding energy of Fe $2p_{3/2}$ electrons located at 710.1 eV and a shoulder at 707.0 ± 0.1 eV which could be assigned to metallic Fe [18,19]. After ion sputtering the spectrum of Fe $2p_{3/2}$ electrons is dominated by the peak belonging to elemental iron (binding energy 707.0 eV). The measured values of binding energies as well as the observed spectral changes on sputtering are consistent with elemental Fe core of nanoparticles covered with Fe-oxide and electrically poorly conducting hydrocarbon polymer shell.

The spectrum of C 1s electrons (Fig. 3b) shows the presence of three components. The main component located at 284.8 eV amounts to about 76% of the total carbon concentration for as received sample and 82% for sputtered sample and belongs to a hydrocarbon polymer (with possible admixture of elemental carbon). Let us mention that the spectrum of the Auger C KLL electrons indicates the presence of predominatly sp^3 hybridized carbon. The minor components of

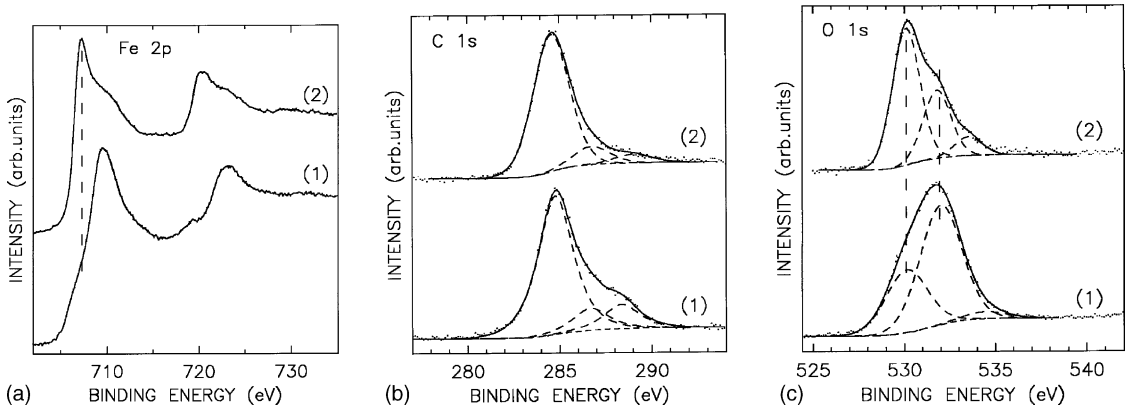

Fig. 3. Spectra of Fe 2p (a), C 1s (b) and O 1s (c) photoelectrons of the powder before (1) and after (2) ion sputtering (the spectra are normalized to the same height).

the C 1s spectra centered at 286.7 eV (approximately 13% of the total C 1s intensity) and 288.9 eV could be assigned to C–OH, C–O–C and O–C=O species, [19] respectively.

The spectra of O 1s electrons (Fig. 3c) contain the component at 530.0 eV, which comes from iron oxide [18] (30% of the total O 1s signal intensity for as received sample and 62% for sputtered sample) and the components from oxygen–carbon functionalities.

The Raman spectra little alter for different examined regions and show the bands at 219, 280, 398 and 490 cm^{-1} assignable [20] to α-Fe_2O_3 together with bands at 676–684, 1335–1380 (D band) and 1585 cm^{-1} (G band) which are due to disordered carbon [21].

The electron diffraction pattern of the powder (Fig. 4) shows a good fit to interlayer distances of crystalline magnetite (Fe_3O_4) and maghemite (α-Fe_2O_3) and provides evidence on the presence of other forms of iron oxides.

The EPR spectra show an intense single line with g-factor of 2.034 and linewidth of 83.8 mT. Both values indicate the presence of Fe^{3+} state. The calculated quantity of iron through double integration of the EPR spectrum yields 2.3×10^{24} spins per gram, which is by more than an order of magnitude higher than the theoretically admissible value. This is compatible with the presence of interaction between magnetic dipoles and considering the symmetry of EPR line with superparamagnetism as prevailing mechanism [22].

The black powder ultrasonically treated in hexane allows formation of a yellow solution whose UV absorption spectrum gradually depletes as the suspended yellow particles slowly descend to the cell bottom. The spectrum (Fig. 5) shows the highest absorption at ~210 nm which continuously tails to 700 nm in a way that absorption at 400 nm is reduced by 50%. We assume that this absorption pattern is mostly due to the carbonaceous shell consisting of nano-sized carbon particles, since it resembles the absorption profile of carbon nanoclusters of different clustering range and shape [23]. We admit, however, that the spectrum can be contributed by a surface plasmon band related to the nano-sized Fe-based core [24].

The measurements of the hysteresis loops and virgin curves were performed in order to specify the magnetic properties at different temperatures. At $T = 5$ K the large coercivity ($H_c = 515$ Oe) indicated a ferromagnetic behaviour occurring below the blocking temperature. The hysteresis loop at $T = 5$ K was also measured under the two different conditions—after cooling in the field 25 and −25 kOe. The

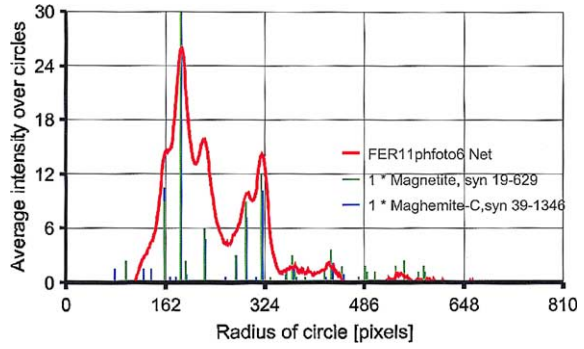

Fig. 4. Diffraction pattern of the powder as compared to that of magnetite and maghemite.

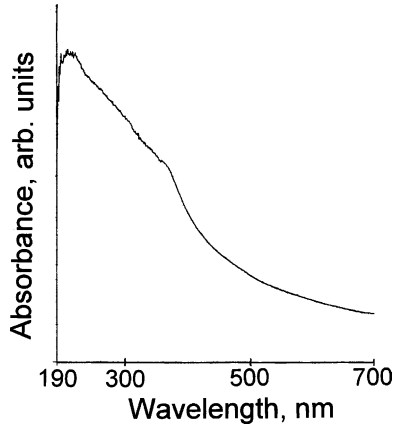

Fig. 5. UV absorption spectrum of the deposited particles in hexane recorded immediately after ultrasonic treatment.

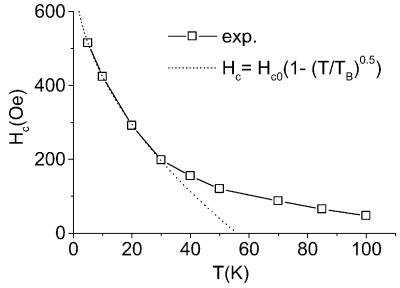

Fig. 6. Temperature dependence of the coercivity H_c and the fit using a $T^{1/2}$ dependence.

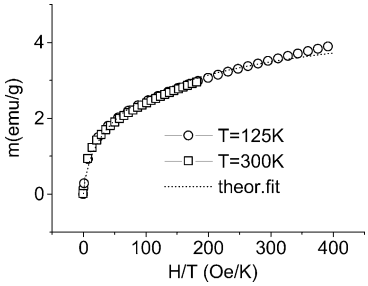

Fig. 8. Measured magnetization at $T = 125$ and 300 K as a function of H/T, a theoretical fit using the Langevin function and log-normal distribution $f(D)$ ($D_0 = 0.326$ nm, $\lambda = 0.7$; λ determines the width of the distribution and D_0 is a diameter corresponding approximately to a maximum of this distribution function [26]).

result shown in Fig. 6 shows an appreciable shift of the loop in the direction, which is opposite to the cooling field. This behaviour suggests the presence of a relatively large unidirectional anisotropy, which can be attributed to an exchange coupling between ferromagnetic and antiferromagnetic (or ferrimagnetic) phases [25]. The ferromagnetic phase is represented by iron particles and the antiferromagnetic (or ferrimagnetic) component by iron oxides (see below).

Towards higher temperatures the hysteresis loops become narrower and the coercivity decreases. In the low-temperature region this dependence can be approximated by the known relation valid for a system of noninteracting particles [25] (Fig. 7), which yields an approximate value of $T_B \approx 55.7$ K. This blocking temperature is usually identified with a temperature T_m, at which the ZFC susceptibility exhibits a maximum. We measured these dependences and found the value of T_m strongly depending on the applied static magnetic field, $T_m \approx 115$ and 44 K for $H = 10$ and 1500 Oe, respectively.

For $T > 120$ K, where the magnetization shows practically no hysteresis we measured the ZFC virgin magnetization curves up to 50 kOe. The $M(H)$ dependences plotted against H/T result approximately in a universal curve (Fig. 8). This shows that for $T > 120$ K the magnetic moment is predominantly given by a superparamagnetic contribution. A small not superparamagnetic rest of the magnetic moment (at $T = 300$ K, we estimate < 0.5 wt.%) arises from randomly formed largest iron particles (e.g. 10 nm). The $M(H/T)$ dependence of a superparamagnetic system is described by the standard Langevin function $L(wH/kT)$ with w denoting the magnetic moment of the superparamagnetic particle. For a spherical particle with diameter D we have $w = (\pi/6)D^3 M_s$,

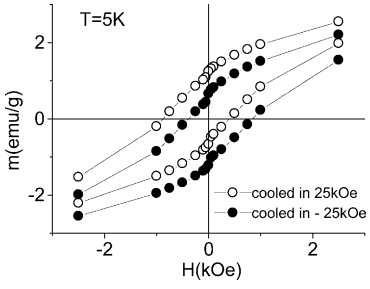

Fig. 7. Central part of the hysteresis loops measured at $T = 5$ K after cooling from $T = 300$ K in the fields 25 and −25 kOe.

where M_s is the bulk saturation magnetization. The $M(H/T)$ curves could not be fitted for a given diameter D but only taking a superposition over a relatively wide range of the diameters D. Using the standard log-normal distribution of the diameters [26], a reasonable fit can be achieved for the average magnetic moment $\langle w \rangle \approx 21.8\mu_B$ and the standard deviation $\Delta w \approx 196.4\mu_B$ (in Fig. 8 by the dotted line).This moment roughly corresponds to 10 iron atoms (contribution $2.2\mu_B$ per atom), so that we can speak rather about iron clusters. The large standard deviation suggests that an appreciable contribution to the magnetic moment arises from the Fe_n ($n \approx 1$ to 100) nanoclusters.

As can be seen, the diameter of the particle (or cluster) depends on the bulk saturation magnetization M_s. If we set $M_s = 1228$ emu/cm^3 for amorphous iron we get that the average moment $21.7\mu_B$ corresponds to the diameter 0.68 nm. This result must be however corrected, since the value of M_s is probably reduced due to an oxidic shell at the surface of the iron particle. The presence of the oxides was also unambiguously proved by a shift of the hysteresis loop. For example for the value of M_s reduced by a factor 8 we obtain two times larger particle diameter, i.e. 1.36 nm ($D \sim M_s^{-1/3}$). Let us remark that this diameter corresponds to the iron core. In the real situation, the particle observed optically in a polymer matrix includes also an oxidic shell having in many cases the diameter several times larger than that of the iron core [27].

In addition to the particle or cluster moment the fitting procedure enables us to determine the saturation magnetization corresponding to the superparamagnetic phase. This yields $M_s \approx 5.6$ emu/g which is near the value of 5.25 as determined by extrapolating the M versus $1/H$ dependence at $T = 125$ K. The quantity M_s is practically independent of temperature. Comparing this value with the bulk saturation magnetization of amorphous iron 158 emu/g, we obtain an effective iron content in the compound equal to 3.5 wt.%, which is much smaller than that estimated on the basis of the chemical analysis. The reason for this disagreement can be attributed to the presence of iron oxides (ferrimagnetic Fe_3O_4 and γ-Fe_2O_3 and especially antiferromagnetic α-Fe_2O_3) that surround ultrafine iron nanoclusters.

4. Conclusion

The ArF laser photolysis of ferrocene in non-polar solvent (hexane) is a slow process with a very low photochemical quantum yield ($<10^{-3}$), which results in the formation of several hydrocarbons and solid nano-sized particles. It is negligibly contributed by the photolytic decomposition of the solvent.

The identified hydrocarbons are multiply unsaturated and aromatic hydrocarbons whose structural identification proves the occurrence of cleavage and polymerization reactions of intermediate cyclopentadienyl radical and cyclopentadiene.

The deposited particles consist of an iron core and oxidized topmost layers, which are composed of iron oxides (γ-Fe_2O_3, α-Fe_2O_3, Fe_3O_4). They are covered with a carbonaceous shell that is composed of both elemental carbon and a polymer that lends the particles their characteristic UV spectrum.

The particles possess interesting magnetic behaviour: they are ferromagnetic at low temperatures ($T = 5$ K) and become superparamagnetic at higher temperature ($T > 120$ K). The detailed analysis of their magnetization behaviour allows to characterize these particles in terms of nanoclusters.

Acknowledgements

This work was supported by the Ministry of Education, Sport and Youth (grant no. ME 611 and OC 523.60) and by Grant Agency of the Academy of Sciences (grant no. A4072107) of the Czech Republic.

References

[1] (a) Y. Nagano, Y. Achiba, K. Kimura, J. Phys. Chem. 90 (1986) 1288;
(b) H.T. Liou, Y. Ono, P.C. Engelking, J.T. Moseley, J. Phys. Chem. 90 (1986) 2888;
(c) U. Ray, H.Q. Hou, Z. Zhang, W. Schwarz, M. Vernon, J. Chem. Phys. 90 (1989) 4248;
(d) S. Niles, D.A. Prinslow, C.A. Wight, P.B. Armentrout, J. Chem. Phys. 97 (1992) 3115.
[2] B.A. Thrush, Nature (London) 178 (1956) 155.
[3] (a) P. Heszler, K. Elihn, M. Boman, J.-O. Carlson, Appl. Phys. A 70 (2000) 613;
(b) K. Elihn, F. Otten, M. Boman, P. Heszler, F.E. Kruis, H. Fissan, J.-O. Carlson, Appl. Phys. A 72 (2001) 29.
[4] (a) E. Koerner von Gustorf, F.-W. Grevels, Fortschr. Chem. Forsch. 13 (1969) 366;
(b) A.M. Tarr, D.M. Wiles, Can. J. Chem. 46 (1968) 2725;
(c) J.A. Powell, S.R. Logan, J. Photochem. 3 (1974) 189.
[5] R.E. Bozak, Adv. Photochem. 8 (1971) 227, and references therein.
[6] (a) L.A. Harris, J.D. Goff, A.Y. Carmichael, J.S. Riffle, J.J. Harburn, T.G.St. Pierre, M. Saunders, Chem. Mater. 15 (2003) 1367, and references therein ;
(b) D.K. Kim, M. Mikhaylova, Y. Zhang, M. Muhammed, Chem. Mater. 15 (2003) 1617.
[7] J.H. Scofield, J. Electron Spectrosc. Relat. Phenom. 8 (1976) 129.
[8] J.L. Lábár, Proceedings of EUREM 12, in: L. Frank, F. Ciampor (Eds.), Czechoslovak Society for Electron Microscopy, Brno, 2000, p. 1379.
[9] JCPDS PDF-2 database, International Centre for Diffraction Data, Newtown Square, PA, U.S.A., release 52, 2002.
[10] (a) S. Sohn, D.N. Hendrickson, H.B. Gray, J. Am. Chem. Soc. 93 (1971) 3603;
(b) A.T. Armstrong, F. Smith, E. Elder, S.P. McGlynn, J. Chem. Phys. 46 (1967) 4321.
[11] J.A. Connor, Top. Curr. Chem. 71 (1977) 71.
[12] M. Heaven, L. Dimauro, T.A. Miller, Chem. Phys. Lett. 95 (1983) 347.
[13] (a) N.J. Turro, G.S. Hammond, J. Am. Chem. Soc. 84 (1962) 2841;
(b) R. Srinivasan, Adv. Photochem. 4 (1966) 128;
(c) J. Miyazaki, Y. Yamada, J. Mol. Struct. 692 (2004) 145, and references therein.
[14] Encyclopedia of Polymer Science and Technology, in: H.F., Mark, N.G., Gaylord, N.M., Bikales (Eds.), Wiley, New York, vol. 4, p. 563.
[15] (a) A. Sabljić, R. McDiarmid, J. Chem. Phys. 93 (1990) 3850;
(b) E.E. van Tamelen, J.I. Brauman, L.E. Ellis, J. Am. Chem. Soc. 93 (1971) 6145.
[16] E. Hedaya, D.W. Mc Neil, P. Schissel, D.J. Mc Adoo, J. Am. Chem. Soc. 90 (1968) 5284.
[17] (a) A. Burcat, M. Dvinyanikov, Int. J. Chem. Kinet. 29 (1997) 505;
(b) G.B. Bacskay, J.C. Mackie, Phys. Chem. Chem. Phys. 3 (2001) 2467.
[18] B.J. Tan, K.J. Klabunde, P.M. Sherwood, Chem. Mater. 2 (1990) 186.
[19] NIST X-ray Photoelectron Spectroscopy Database, ver. 2.0, US Department of Commerce, NIST, Gaithersburg, MD 20899, USA, 1997.
[20] (a) L.J. Oblonsky, T.M. Devine, Corros. Sci. 37 (1995) 17;
(b) M.I. Baraton, G. Busca, M.C. Priieto, G. Ricchiardi, V. Sanchez Escribano, J. Sol. State Chem. 112 (1994) 9.
[21] (a) A.C. Ferrari, J. Robertson, Phys. Rev. B 61 (2000) 14095;
(b) J. Schwan, S. Ulrich, V. Batori, H. Ehrhard, J. Appl. Phys. 80 (1996) 440, and references therein ;
(c) V. Vorlíček, P. Široký, J. Sobota, V. Peřina, V. Železný, J. Hrdina, Diamond Relat. Mater. 5 (1996) 570.
[22] C.T. Hseih, V.L. Huang, J.T. Lue, J. Phys. Chem. Solids 63 (2002) 733.
[23] M. Schnaiter, H. Mutschke, J. Dorschner, T. Henning, F. Salama, Astrophys. J. 498 (1998) 486, and references therein.
[24] (a) C.F. Bohren, D.R. Huffman, Absorption and Scattering of Light by Small Particles, Wiley, New York, 1983;
(b) Y.-S. Shon, S.M. Gross, B. Dawson, M. Porter, R.W. Murray, Langmuir 16 (2000) 6555, and references therein ;
(c) Y. Takeda, C.G. Lee, N. Kishimoto, Nucl. Instrum. Methods Phys. Res. 190 (2002) 797.
[25] F.C. Fonseca, G.F. Goya, R.F. Jardim, R. Muccillo, N.V. Carreno, E. Longo, E.R. Leite, Phys. Rev. B 66 (2002) 104406.
[26] C. Caizer, Physica B 327 (2003) 27.
[27] N.A.D. Burke, H.D.H. Stover, F.P. Dawson, Chem. Mater. 14 (2002) 4752.